

Short Communication

Effect of welding parameters on microstructure and mechanical properties of AA6061-T6 butt welded joints by stationary shoulder friction stir welding



Dongxiao Li, Xinqi Yang*, Lei Cui, Fangzhou He, Hao Shen

Tianjin Key Laboratory of Advanced Joining Technology, School of Materials Science and Engineering, Tianjin University, Tianjin 300072, People's Republic of China

ARTICLE INFO

Article history:

Received 29 May 2014

Accepted 22 July 2014

Available online 31 July 2014

ABSTRACT

Stationary shoulder friction stir welding (SSFSW) butt welded joints were fabricated successfully for AA6061-T6 sheets with 5.0 mm thickness. The welding experiments were performed using 750–1500 rpm tool rotation speeds and 100–300 mm/min welding speeds. The effects of welding parameters on microstructure and mechanical properties for the obtained welds were discussed and analyzed in detail. It is verified that the defect-free SSFSW welds with fine and smooth surface were obtained for all the selected welding parameters, and the weld transverse sections are obviously different from that of conventional FSW joint. The SSFSW nugget zone (NZ) has “bowl-like” shapes with fairly narrow thermal mechanically affected zone (TMAZ) and heat affected zone (HAZ) and the microstructures of weld region are rather symmetrical and homogeneous. The 750–1500 rpm rotation speeds apparently increase the widths of NZ, TMAZ and HAZ, while the influences of 100–300 mm/min welding speeds on their widths are weak. The softening regions with the average hardness equivalent 60% of the base metal are produced on both advancing side and retreating side. The tensile properties of AA6061-T6 SSFSW joints are almost unaffected by the 750–1500 rpm rotation speeds for given 100 mm/min, while the changing of welding speed from 100–300 mm/min for given 1500 rpm obviously increased the tensile strength of the joint and the maximum value for welding parameter 1500 rpm and 300 mm/min reached 77.3% of the base metal strength. The tensile fracture sites always locate in HAZ either on the advancing side or retreating side of the joints.

© 2014 Elsevier Ltd. All rights reserved.

1. Introduction

Friction stir welding (FSW) which was developed by TWI in 1991 is a relatively mature solid joining technology for aluminum alloys and has been successfully applied in many industrial sectors with various joint configurations [1–6]. Stationary shoulder friction stir welding (SSFSW) is an alternative approach of FSW and was primarily invented by TWI to weld low thermal conductivity Ti-6Al-4V [7]. SSFSW consists of a rotating pin and a non-rotating shoulder, which frictionally slides over the surface of the material during welding [8].

In conventional FSW, the rotational shoulder is believed to generate the majority of frictional heat during the welding process [9]. While in SSFSW, the shoulder is static and no longer acts as a stir component generating frictional heat. The rotational pin produces almost linear heat input throughout the welding [10], and the asymmetrical microstructure and properties of the weld caused

by conventional FSW tool are reduced [11]. Besides, stationary shoulder creates a smooth weld surface appearance with no cross section reduction [10]. SSFSW can be easily applied for welding butt joints with different thickness and corner joints. So, it attracted more and more attentions in industrial fields.

SSFSW is one of the advanced solid-state joining technologies, and currently there are only a few open literatures published on SSFSW because of technical confidentiality. Davies et al. studied the crystallographic texture and microstructure of a SSFSW Ti-6Al-4V weld in detail [12]. Ahmed et al. investigated the through-thickness crystallographic texture of a SSFSW aluminum weld joint. They concluded that the use of SSFSW reduced the shoulder-affected region and that the stationary shoulder only affected a very thin surface layer at the top of the weld [11]. Widener et al. successfully performed AA6061-T6 welding experiments under very high rotation rate using SSFSW, and it was found that SSFSW could apparently improve the surface forming of the weldment and reducing weld defects [13]. Martin et al. reported the application of SSFSW on aluminum corner joint and found that SSFSW corner joint had more advantages than conventional FSW

* Corresponding author. Tel.: +86 022 27406261; fax: +86 022 27407022.

E-mail address: xqyang@tju.edu.cn (X. Yang).

corner joint [8]. YU performed paralleled double-pass lap joints for aluminum 7075-T6. The effect of welding control parameters and tool geometry on welding process were investigated. The microstructure, distortion and mechanical properties were studied. They found that SSFSW joint are of fewer defects and has a higher UTS compared to conventional FSW joint [14].

In order to understand mechanism of SSFSW process, Merlin performed both numerical and experimental investigation of the thermal cycle during the butt joint welding of aluminum 2024 using SSFSW [15]. Liu and his co-workers studied the microstructure and the effect of welding speed and tool rotation speed on the mechanical properties of 2219-T6 aluminum welds made by external non-rotation shoulder assisted FSW. They found that the microstructure and hardness profile of the joints are asymmetrical, and the defect-free joint could be obtained when rotation speeds are in the range of 600–900 rpm and the maximum tensile strength of joint could reach 69% of base metal strength for 800 rpm. However, the tool still has a small rotational shoulder and the weld structure is similar to that made by using conventional FSW [16,17]. Up to now the published literatures on SSFSW seldom reported in detail the influence of welding parameters on the microstructure and mechanical properties of the SSFSW welded joint.

In order to develop and promote the application of the advanced SSFSW technology, a SSFSW tool package was developed independently and installed on the special FSW machine. The welding experiments of SSFSW butt joints for AA6061-T6 sheets were performed using 750–1500 rpm tool rotation speeds and 100–300 mm/min welding speeds, and the influences of welding parameters on weld forming, microstructure, hardness, and mechanical properties during SSFSW process for AA6061-T6 base metal were discussed and analyzed thoroughly. These research results provide the important bases to understand the SSFSW features.

2. Experimental procedures

The base material used in this study was 5 mm 6061-T6 aluminum alloy sheet. The nominal chemical compositions and the tensile properties are listed in Table 1. The welded sheet was cut to the dimension of 320 × 105 mm. Welding was carried out parallel to the rolling direction of the sheets using the special FSW machine equipped with SSFSW tool package. The welding parameters used in this study are summarized in Table 2. The upset forging pressure of tool package are approximately kept constant during SSFSW process.

The stationary shoulder and tool used in the experiments were developed independently and installed on the spindle head of FSW machine, and the structures are illustrated in Fig. 1. The tool employs a conical-threaded probe design with the bottom diameter of 8 mm and the top diameter of 5 mm. The probe protruding length and the diameter of the stationary shoulder are 4.9 mm and 16 mm, respectively. During the welding process, the tool was operated with a back tilt angle of 2.5 degree.

All the SSFSW testing sheets were cross sectioned perpendicular to the welding direction according to the standard AWS D 17.3 [18] to make the metallographic observing specimens. The appearances of weld surfaces were visually estimated and taken photos by

Table 2
Welding parameters of SSFSW AA6061-T6 joints.

Sample	Tool rotation speed (rpm)	Welding speed (mm/min)
1	750	100
2	1000	100
3	1250	100
4	1500	100
5	1500	200
6	1500	300

digital camera Cannon EOS 600D. Metallographic specimens were ground and polished, then etched using modified Keller's reagent. Macro- and microstructure observations of the welds were performed using optical microscopy Olympus GX51. TEM specimens were cut from the HAZ and NZ using Electric spark cutting machine, ground by abrasive paper and processed by dual jet electrolytic polishing machine. The coarse second phase particles and fine precipitates were examined using SEM Hitachi S-4800 and TEM Tecnai G2 F20, respectively.

The hardness measurements were made on metallographically prepared specimens by Wilson 432SVD hardness gauge using a 300 g load and a dwell time of 10 s. The hardness distribution of the weld obtained using tool rotation speed of 1000 rpm and welding speed of 100 mm/min was measured in 500 μm × 500 μm arrays (as is shown in Fig. 2) covering the transverse section to reveal the typical hardness profiles. For the other specimens obtained under various tool rotation speeds and welding speeds, hardness points were measured only on the mid-thickness line of the joint transverse section in 500 μm step to illustrate the influence of welding parameters on the hardness distribution.

To evaluate the mechanical properties of the welds, three tensile specimen duplicates for each weldment were prepared according to standard ASTM: E8. Static tensile tests were performed using CSS-44100 universal testing machine with the loading speed of 2 mm/min. After tensile tests, the typical fractography were observed using SEM Hitachi S-4800. Besides, a pair of fractured specimens for each welding parameter were mounted in an epoxy mold and implemented to grinding and polishing followed by etching. Then, the fracture position was examined by Optical Microscopy Olympus GX51.

3. Results and discussions

3.1. Weld appearance and transverse section macrograph

The appearance of the weld made using 750 rpm and 100 mm/min is shown in Fig. 3. The surface is fine and smooth with an existing hole at the end and only a piece of burr at the beginning of the weld seam. The width of the welding mark is equivalent to the diameter of the stationary shoulder. The stationary shoulder prevented the stirred material at the welding zone escaping to form burrs. Thus, stationary shoulder helps to get a smooth and fine surface which does not need to be further machined. In addition, the good formability of SSFSW welds is potentially beneficial to the fatigue property.

The surface appearances of the joints made using different welding parameters are illustrated in Fig. 4. It can be seen that

Table 1

Nominal chemical compositions and tensile properties of base material AA6061-T6.

Chemical composition, mass fraction						Mechanical properties	
Si	Fe	Cu	Mn	Mg	Al	UTS (MPa)	EI (pct.)
0.4–0.8	0.7	0.15–0.40	0.15	0.8–1.2	Balance	331	11.7

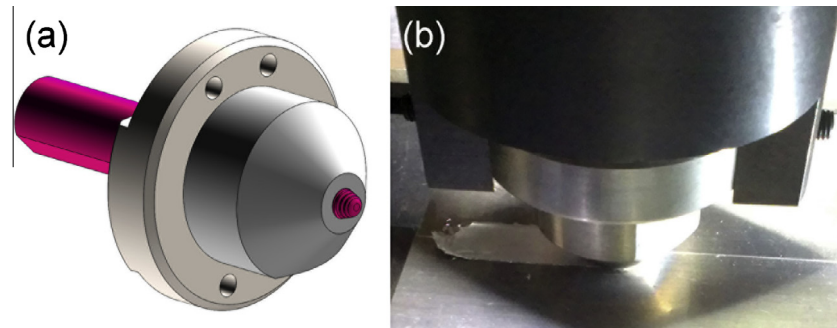


Fig. 1. Stationary shoulder and tool: (a) schematic view and (b) picture of the welding process.



Fig. 2. Schematic for hardness measurement.

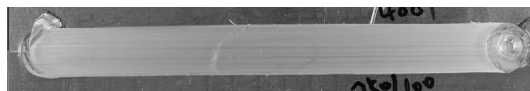


Fig. 3. The appearance of the weldment obtained at the rotation speed of 750 rpm and welding speed of 100 mm/min.

the welding parameters made little difference on the surface appearance of the welds.

Fig. 5(a) and (b) shows the macrostructures of transverse sections for SSFSW joint and conventional FSW joint [19], respectively. The joint shown in **Fig. 5(b)** was made by conventional FSW at the revolutionary pitch of 0.13 mm/r [19], which is equivalent to the welding parameter (100 mm/min and 1000 rpm) used for the SSFSW joint shown in **Fig. 5(a)**. The shoulder and probe diameters for the joint in **Fig. 5(b)** are 15 mm and 6 mm,

respectively. For the SSFSW joint shown in **Fig. 5(a)**, the shape of the weld nugget zone (NZ) is basically bowl-like. The shape is mainly caused by the conical-threaded probe profile. So, if a cylinder-shaped probe was used the weld nugget may be symmetrical and distortion asymmetry could be avoided. Further investigation of the influence of the probe shape on the weld properties is necessary. Comparing **Fig. 5(a)** with (b), it can be found that the macrostructures of the two joints are of great difference. With similar shoulder diameter, joint made by conventional FSW has a large TMAZ and an asymmetry weld nugget, while joint made by SSFSW has no visible TMAZ and a fairly narrow HAZ and a much more symmetric weld nugget.

The transverse section macrographs for SSFSW joints made using various tool rotation speeds and various welding speeds are shown in **Figs. 6 and 7**, respectively. It can be observed that all joints show bowl-shaped NZ with different width. The widths of NZ and HAZ are greatly influenced by the tool rotation speed and the welding speed. The width of NZ and HAZ increase with the increasing of tool rotation speed and decrease with the increasing welding speed. When a constant welding speed is employed, high tool rotation speed created a large heat input and severe plastic flow. Contrarily, when the tool rotation speed is constant, high welding speed causes a small heat input and less plastic flow. However, the NZ and HAZ widths are influenced much more by the tool rotation speed than the welding speed.

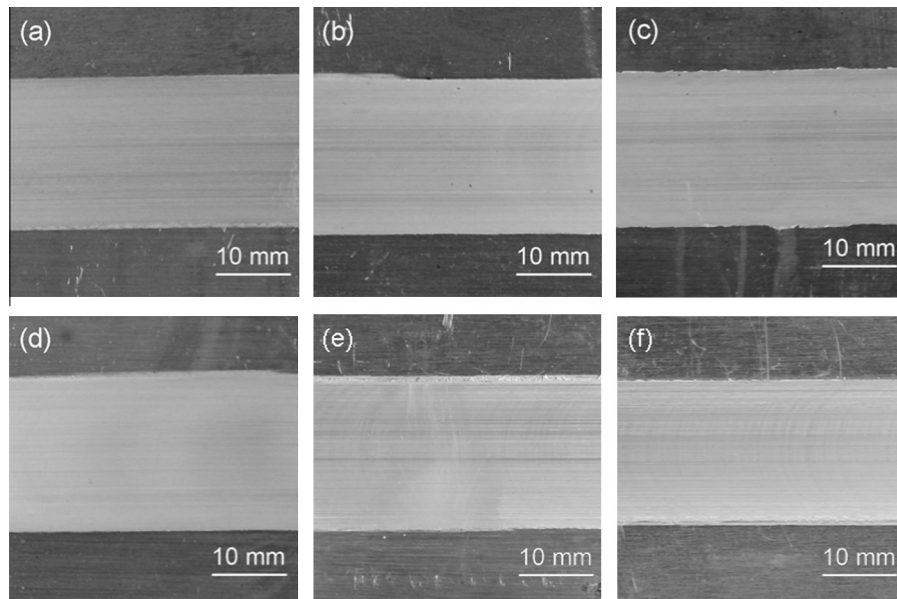


Fig. 4. Surface appearance for the welds obtained at various welding parameters: (a) 750 rpm and 100 mm/min, (b) 1000 rpm and 100 mm/min, (c) 1250 rpm and 100 mm/min, (d) 1500 rpm and 100 mm/min, (e) 1500 rpm and 200 mm/min, and (f) 1500 rpm and 300 mm/min.

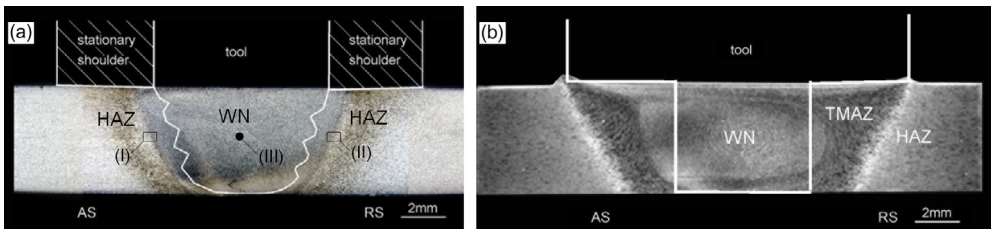


Fig. 5. Transverse section macrostructures for SSFSW joint (a) and conventional FSW joint (b) [19].

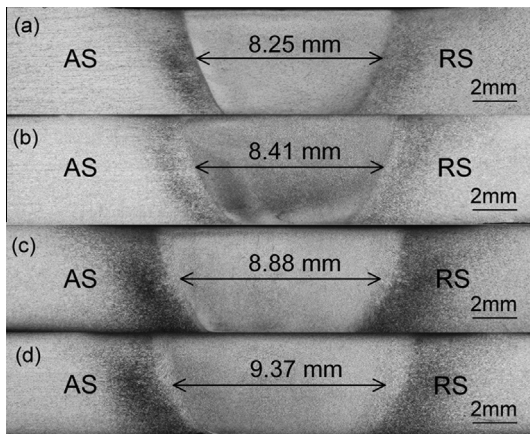


Fig. 6. Transverse section macrographs for the joints obtained at the welding speed of 100 mm/min: (a) 750 rpm, (b) 1000 rpm, (c) 1250 rpm, and (d) 1500 rpm.

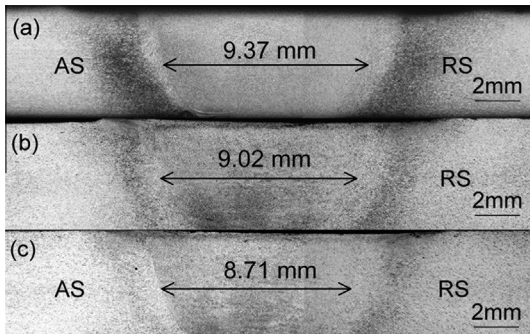


Fig. 7. Transverse section macrographs for the joints obtained at the tool rotation speed of 1500 rpm: (a) 100 mm/min, (b) 200 mm/min, and (c) 300 mm/min.

3.2. Microstructure

Fig. 8 shows the microstructures for NZ borders on AS and RS (indicated by (I) and (II) in Fig. 5(a)) of weld joints made using different parameters. For the weld joint made using 1000 rpm and 100 mm/min, the TMAZ can be observed on AS with a width of about 200 μm . But no TMAZ can be observed on RS. For the joint made using 1500 rpm and 100 mm/min, TMAZ can be seen on both AS and RS with a maximum width of about 300 μm . The deformation of the material on AS are more severe than on RS. For the joint made using 1500 rpm and 300 mm/min, evident TMAZ locates on AS and the material on RS are rarely deformed, which is similar to the microstructure of the joint made using 100 mm/min and 1000 rpm. For all the joints, the width of TMAZ are larger on AS than on RS.

For the given welding speed of 100 mm/min, the TMAZ of the weld obtained using high rotation speed is wider than that of the weld obtained using low rotation speed either on AS or RS. In

addition, the width of TMAZ on both AS and RS are narrower for the weld made using high welding speed than using low welding speed for the given rotation speed of 1500 rpm. So, the width of TMAZ are influence by either tool rotation speed or welding speed. This is caused by various energy input resulting from various welding parameters. With large energy input, the material at TMAZ become soft and get deformed easily by the material flow at NZ borders. This indicates that the energy input increases with the increasing of tool rotation speed and the decreasing of welding speed.

Fig. 9 shows the micrographs for NZ of SSFSW weld joints made using different welding parameters. All the NZ are characterized by fine equiaxed grains with different sizes, which are generated by recrystallization in the welding process. The grain size variation is caused by the weld temperature field and different cooling rate. With high temperature and slow cooling rate, the recrystallized fine equiaxed grains grow bigger. However, the cooling rate for the three welds are considered to be almost the same. So, comparing Figs. (a), (b) and (c) in Fig. 9, it can be inferred that the temperature for the weld shown in Fig. 9(b) was the highest among the three welds. Therefore, either high tool rotation speed or low welding speed results in a high welding temperature in weld NZ.

Fig. 10 shows the secondary electron (SE) micrographs for different locations of SSFSW joint obtained using tool rotation speed of 1000 rpm and welding speed of 100 mm/min. The holes in Fig. 10 are caused by the corrosion of the coarse second phase particles by the acid aqueous solution used for revealing the microstructure. So, these holes present for the location and distribution of the coarse second phase particles. The coarse second phase particles in Al–Mg–Si alloy system are -Mg₂Si [20,21]. Fig. 10(a) is the base material of aluminum 6061 heat treated with the T6 condition. Little coarse second phase particles are observed and the main strengthening particles are fine precipitates which are hardly to see on SE micrographs. HAZ shown in Fig. 10(b) shows a surface with a large amount of second phase particles. Fig. 10(c) and (d) shows the morphology of TMAZ and NZ, respectively. Evidently material flow can be observed in TMAZ. The second phase particles in TMAZ are smaller than in HAZ. NZ consists of fine equiaxed grains and small second phase particles. The existence small holes in NZ implies that the heat input is inadequate to totally solve the second phase particles.

Fig. 11 shows the precipitates in different locations of SSFSW weld made using 1000 rpm and 100 mm/min. The NZ is mainly characterized by small dots which are supposed to be GP-I zones. It is indicated that the premier precipitates in the 6061-T6 alloy are dissolved in the welding process and these dot-like precipitates reprecipitate homogenously in the follow cooling. While HAZ shows a typical Widmanstätten pattern structure. Long needle-like precipitates and short rod-like precipitates are present in certain orientations in the vision. In addition, few plate-like precipitates can be observed. The base material is supposed to contain a high density of fine needle-like precipitates which are the main source of strengthening. In the HAZ, the needle-like precipitates grow and transformed into short rod-like precipitates as a result of the

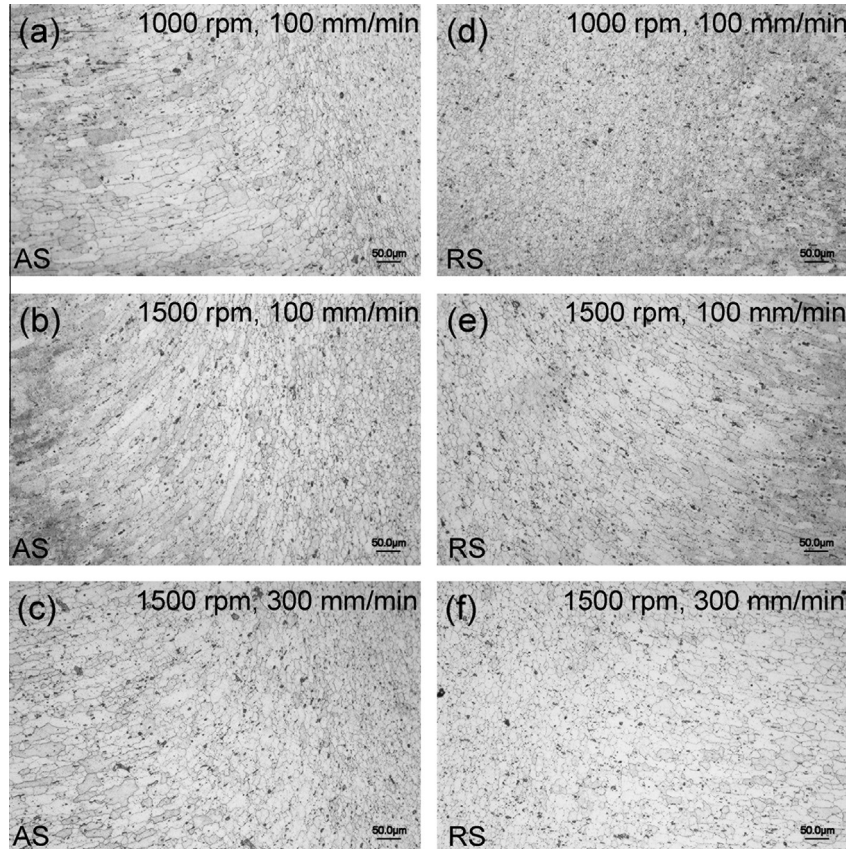


Fig. 8. Enlarged micrographs for the locations indicated by (I) and (II) in Fig. 5(a) of different welds on AS and RS: (a) and (d) 1000 rpm and 100 mm/min, (b) and (e) 1500 rpm and 100 mm/min, (c) and (f) 1500 rpm and 300 mm/min.

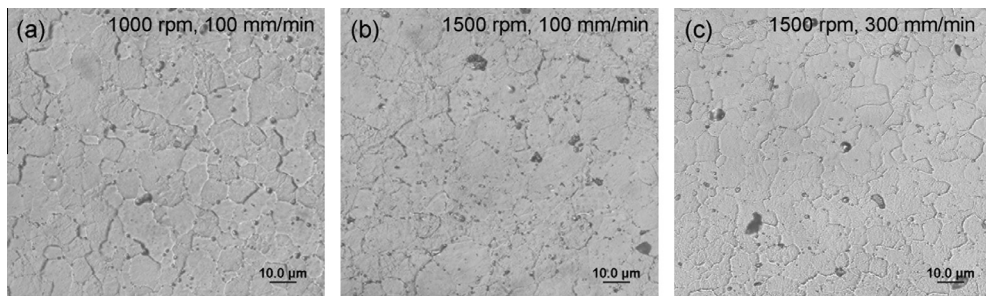


Fig. 9. Micrographs for NZ of SSFSW weld joint made using various tool rotation speeds and welding speeds: (a) 1000 rpm and 100 mm/min, (b) 1500 rpm and 150 mm/min, and (c) 1500 rpm and 300 mm/min.

thermal circle of the welding. The coarse second phase particles and fine precipitates in Al-Mg-Si alloy system have been widely discussed in the earlier work. According to these previous researches, the coarse second phase particles in Fig. 10 are β -Mg₂Si; the fine dot-like precipitates in Fig. 11(a) are GP zones; the needle-like and rod-like precipitates are β'' and β' , respectively [20–22].

3.3. Hardness distribution

Fig. 12 shows the transverse section micro-hardness profile of 6061-T6 SSFSW butt joint made using rotation speed of 1000 rpm and welding speed of 100 mm/min. The hardness profile shows a significant decrease compared to 100–110 HV at the base material. The regions near the NZ borders on both AS and RS showed a severe softening behavior with the hardness ranging

from 50–75 HV. The hardness of the upper part of NZ is relatively high and has a hardness of about 80 HV. The width of the severe softening region on AS is evidently wider than that on RS. Meanwhile, the bottom of NZ is softer than the top.

It is known that AA6061 contains various strengthening precipitates such as the GP-I zones, GP-II zones (or β''), and β -Mg₂Si [18–21]. During the welding process, both dissolution and growth of the precipitates which are mentioned above occur due to the heat cycle. The high density of fine needle shaped β'' precipitate is the main strengthening source for AA6061-T6, but it is a metastable transient phase and may be dissolved and evolve to β' and β -Mg₂Si phase during the welding.

It is likely that the β'' precipitates in the middle part of NZ (marked I in Fig. 12) are dissolved by the heat generated in the welding process. Consequently, GP zones precipitate in the following cooling of the weld. Thus, the softening of NZ occurred.

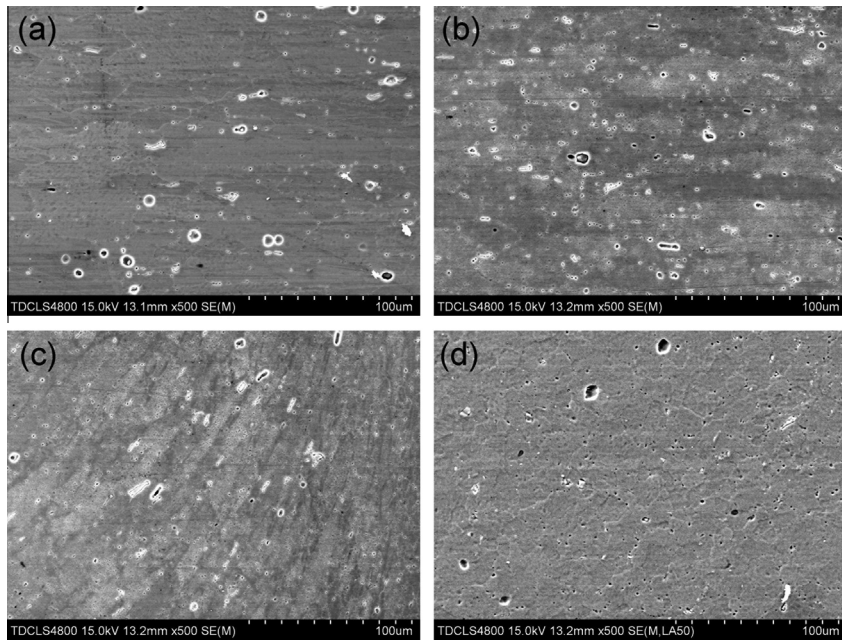


Fig. 10. Secondary electron micrograph for different locations of SSFSW joint obtained using tool rotation speed of 1000 rpm and welding speed of 100 mm/min: (a) base material, (b) HAZ, (c) TMAZ, and (d) NZ.

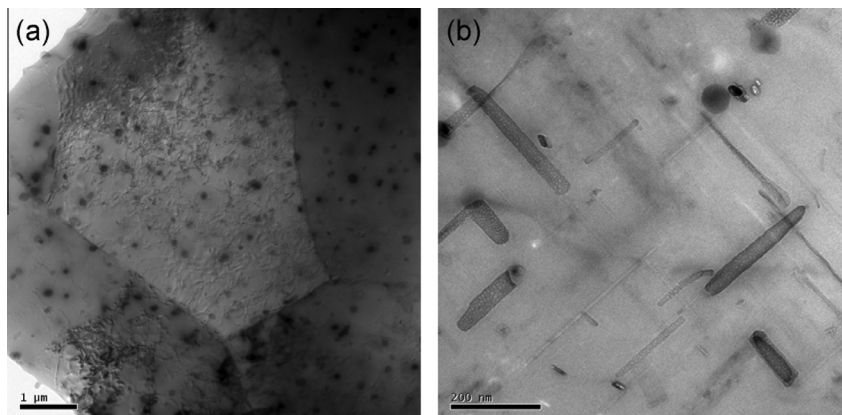


Fig. 11. TEM micrographs for different locations of the weld made using tool rotation speed of 1000 rpm and welding speed of 100 mm/min: (a) NZ, (b) HAZ.

Nevertheless, the bottom region of NZ (marked II in Fig. 12) cooled down too rapidly for the precipitation of GP zones due to a quick heat transfer of the anvil. This may result in the even softer region at the bottom of NZ (marked II in Fig. 12). The region marked III in Fig. 12 are at the borders of NZ on AS and RS respectively. This region shows a strongly softening feature. Region III experienced fairly high temperature which caused the overaging of the material. The regions marked IV in Fig. 12 are supposed to contain fine β'' , coarsened β' precipitates and GP zones and showed a slightly softened behavior comparing to the parent material. However, these discussions are based on the TEM micrographs in Section 3.2 and previous works focusing on the microstructure evolution during FSW [20–25]. Further work is needed to assert the softening mechanism of SSFSW joint in detail.

Figs. 13 and 14 show the hardness profile on the mid-thickness line for the welds obtained at different tool rotation speeds with the welding speed of 100 mm/min and different welding speeds with tool rotation speed of 1500 rpm, respectively. The probe and NZ diameters at the mid-thickness line for all the welds are illustrated in Figs. 13 and 14. The hardness values in NZ and HAZ

decreased at different degrees. The softest region locates in HAZ for all the welds. At the welding speed of 100 mm/min, the NZ hardness are higher at high tool rotation speeds (1250 rpm and 1500 rpm) than at low tool rotation speeds (750 rpm and 1000 rpm). This indicates that more strengthening precipitates generated at high tool rotation speeds. The lowest hardness in HAZ for the welds obtained at the same welding speed ranges from 55–60 HV. Under constant welding speed of 100 mm/min, the width of most softened regions in HAZ at mid-thickness line for the joints made using low tool rotation speeds (750 rpm and 1000 rpm) are wider at AS than at RS. While this phenomenon are to the contrary for the joints made using high tool rotation speeds (1250 rpm and 1500 rpm). The width of the region where the hardness degraded seriously increases with the increasing of tool rotation speed. For the given tool rotation speed, the hardness in NZ seems to be fluctuating, especially for the welds made using welding speeds of 200 and 300 mm/min. The lowest hardness in HAZ for all three joints are of little difference (about 60 HV). The width of the region where the hardness degraded most decreases with the increasing welding speed. So, the width of the

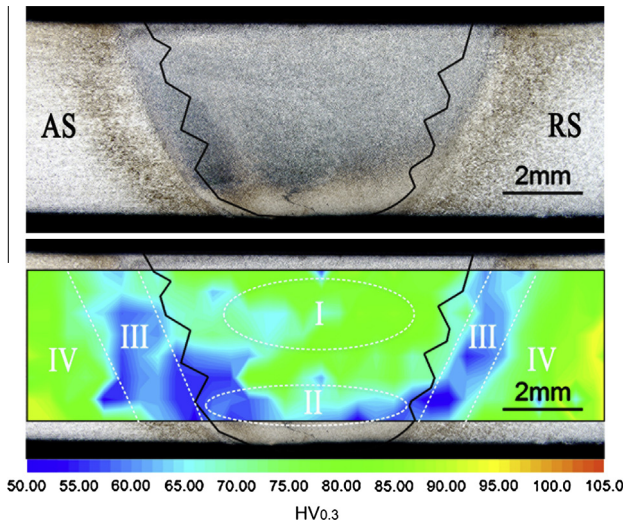


Fig. 12. Hardness distribution on the transverse section of the weld obtained at the welding speed of 100 mm/min and rotation speed of 1000 rpm.

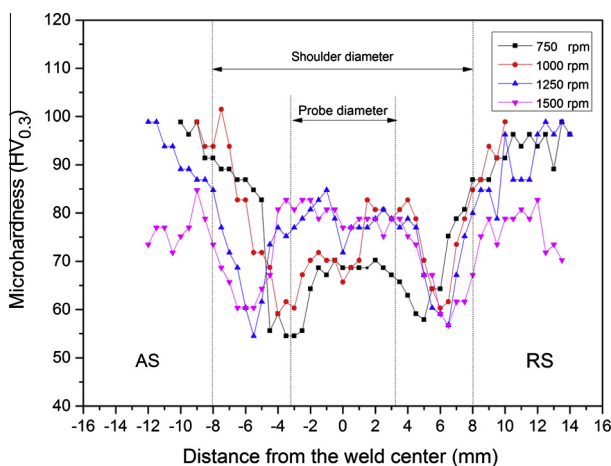


Fig. 13. Hardness profile on the mid-thickness line of SSFSW welds made using various tool rotation speeds and welding speed of 100 mm/min.

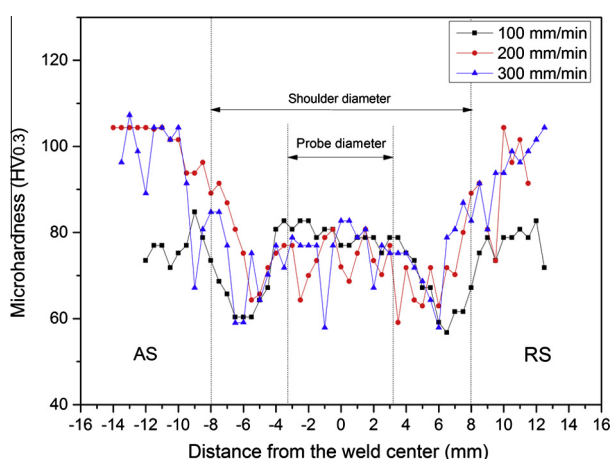


Fig. 14. Hardness profile on the mid-thickness line of SSFSW welds made using various welding speeds and tool rotation speed of 1500 rpm.

hardness-degraded region is influenced by both welding speed and tool rotation speed. The lowest value of hardness in the weld are effected by mainly by the tool rotation speed.

3.4. Tensile tests and fracture characteristics

The effects of tool rotation speed and welding speed on the ultimate tensile strength and elongation are shown in Figs. 15 and 16, respectively. When the tool rotation speed varies from 750 to 1500 rpm with the welding speed of 100 mm/min, the tensile strength keeps almost constant, varying from 217 to 219 MPa. The elongation is slighter larger at higher rotation speed of 1250 and 1500 rpm. However, the tensile properties are not sensitive to the tool rotation speed for the welding speed of 100 mm/min. For the weld joints made using tool rotation speed of 1500 rpm and different welding speeds, the UTS increases with the increasing of welding speed. The maximum joint efficiency of 77.3% (256 MPa) was achieved using 1500 rpm and 300 mm/min. The elongation at the welding speed of 100 mm/min is larger than that at the welding speed of 200 mm/min and 300 mm/min. The tensile fracture of all the obtained welds locates in HAZ either on AS or RS (as is shown in Figs. 17 and 18). So the tensile properties are dominated by the microstructure of HAZ which is mainly featured by the type and density of fine precipitates. The heat cycle in SSFSW process causes the evolution of the fine precipitates and influences the mechanical property. Over aging which is caused by high temperature and long holding time during the heat cycle can greatly reduce the UTS and hardness. From Figs. 15 and 16, it is suggested that low welding speed causes serious over aging of HAZ and low UTS. While, tool rotation speed makes little influence on the precipitates in HAZ. In general, the tensile properties of SSFSW joint are greatly influenced by the welding speed for the tool rotation speed of 1500 rpm and are hardly influenced by the tool rotation speed for the welding speed of 100 mm/min.

In conventional FSW, it is reported that tool rotation speed (87–342 mm/min) and welding speed (1250–3600 mm/min) both make no significant influence on the tensile properties of AA6061-T6. The UTS keep approximately 200 MPa [22]. This suggests that heat input in conventional FSW is fairly high regardless of the tool rotation speed and welding speed. However, in SSFSW the heat input can be eliminated at a rather low degree and the base material can maintain unaffected to a large extent.

Figs. 17 and 18 show the fracture locations of SSFSW butt welds made using the welding speed of 100 mm/min with different tool rotation speeds and at the tool rotation speed of 1500 rpm with

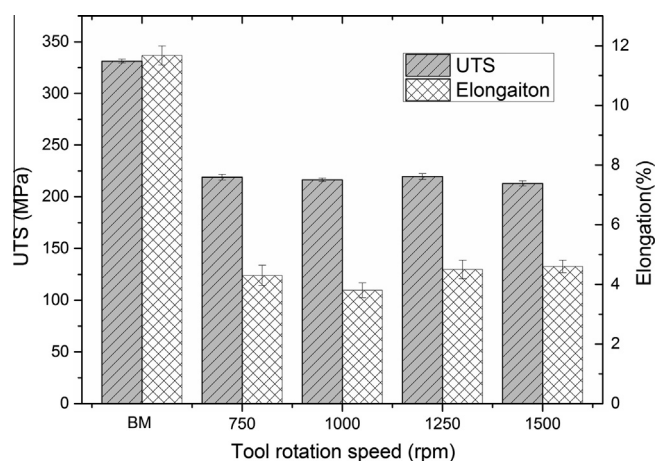


Fig. 15. Tensile properties of SSFSW welds at the welding speed of 100 mm/min and various tool rotation speeds.

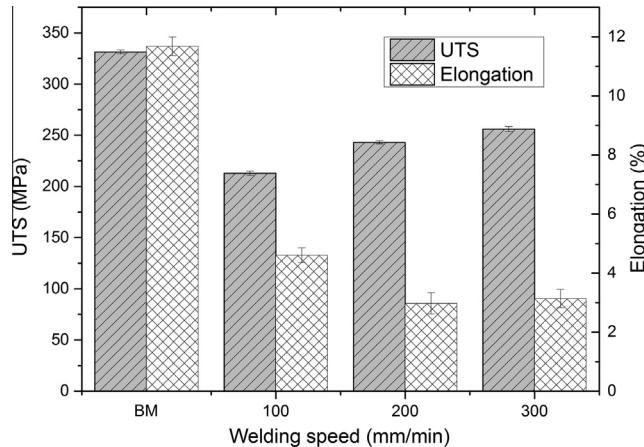


Fig. 16. Tensile properties of SSFSW welds at the tool rotation speed of 1500 rpm and various welding speeds.

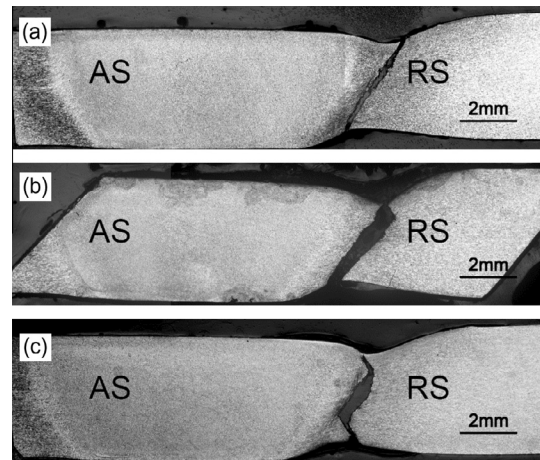


Fig. 18. Fracture location of SSFSW welds at the tool rotation speed of 1500 rpm with different welding speeds: (a) 100 mm/min, (b) 200 mm/min, and (c) 300 mm/min.

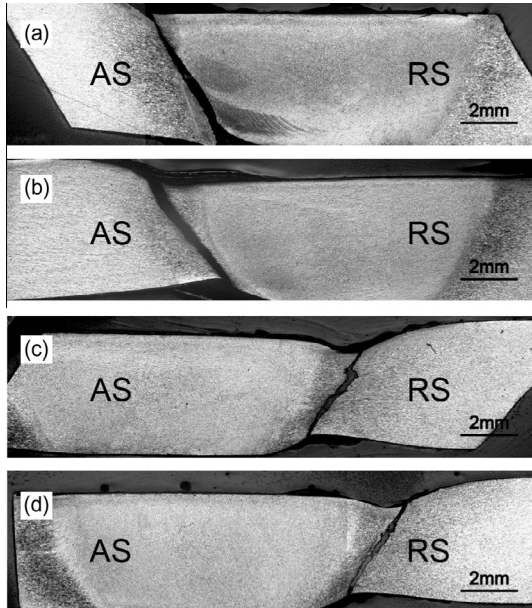


Fig. 17. Fracture location of SSFSW welds at the welding speed of 100 mm/min with different tool rotation speed: (a) 750 rpm, (b) 1000 rpm, (c) 1250 rpm and (d) 1500 rpm.

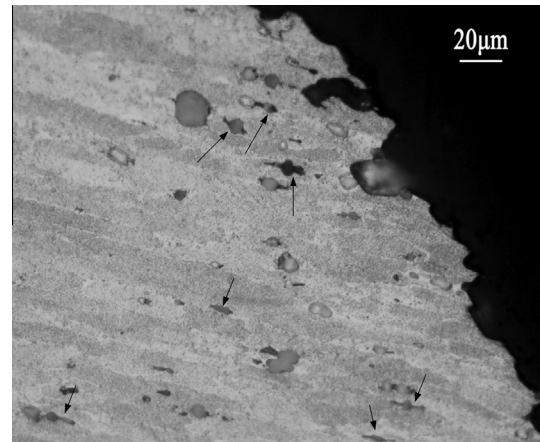


Fig. 19. Micrograph showing the origins of cracks.

arrows in Fig. 19, the material surrounding the coarse second phase particles are teared out in the tensile test. When tensile stress was applied, plastic strain localized mainly in the weakest zone at HAZ, where the second phase particle coarsened most during the heat cycle in the welding process, and subsequent caused necking. Because high strain hardening capacity of NZ [24] and high true stress at the necking area, continuous plastic strain took place at the necking area. Furthermore, the coarse second phase particles are absolute incoherent with the α -Al lattice. So, the material surrounding the coarse second phase particles are teared out and micro voids nucleates at these sites. With the increasing stress, the micro voids grow, coalesce and eventually form a continuous fracture surface.

The fracture surface of the weld made using 100 mm/min and 1000 rpm is shown in Fig. 20. The fractography is dominated by ductile transgranular failure, which is characterized mainly by the fully dimpled rupture surface. Typical elongated dimples with various sizes are the result of localized strain continuity caused by second phase particles which had coarsened after the welding process. Thus, the fracture is closely relative with the coarse second phase particles which has been discussed in Section 3.2 (as is shown in Fig. 10).

different welding speeds. Except for the joint shown in Fig. 17(a), all the joints fractured at the HAZ either on AS or RS. For FSW joints, it is widely accepted that the tensile failure is likely to occur at the location with minimum hardness profile for heat treatable aluminum. The locations of the fracture of SSFSW joints represented in this paper imply that the increasing tool rotation speed causes a change in the temperature distribution which is the direct cause of the hardness profile in the weld joint. The tensile fracture for FSWed heat treatable aluminiums usually occurs in HAZ due to the severe overaging in this region [16,19,21]. And the fracture location in this paper is consistent with the early works on conventional FSW.

Fig. 19 shows the microstructure of the fractured weld joint near the main crack path. The holes in Fig. 19 are caused by the corrosion of the coarse second phase particles by the acid aqueous solution used for revealing the microstructure. As indicated by the

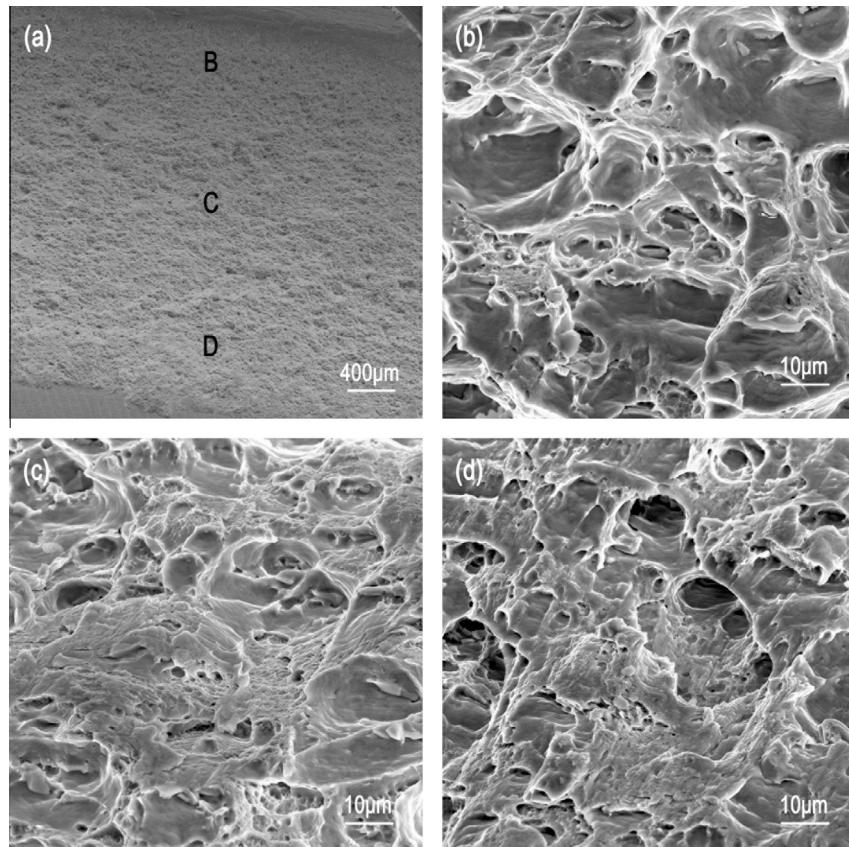


Fig. 20. Fractography of SSFSW weld obtained using welding speed of 100 mm/min and tool rotation speed of 1000 rpm: (a) macrograph, (b–d) show the locations marked B, C and D in Fig. 20(a), respectively.

4. Conclusions

The welding experiments of SSFSW butt joints for AA6061-T6 sheets were performed using various welding parameters and the influences of welding parameters on the properties of SSFSW welds were investigated. The main conclusions are listed as follows:

- (1) SSFSW butt welded joints for 5.0 mm thickness of AA6061-T6 sheets were successfully performed and defect-free SSFSW welds with fine and smooth appearance were obtained for all the selected welding parameters of 750–1500 rpm tool rotation rates and 100–300 mm/min welding speeds.
- (2) The weld transverse sections of AA6061-T6 SSFSW joints are obviously different from that of conventional FSW joint. The NZ of AA6061-T6 SSFSW joint has bowl-like shape with narrower TMAZ and HAZ and the microstructures of weld region are more symmetrical and homogeneous. The 750–1500 rpm tool rotation speeds apparently increase the widths of NZ, TMAZ and HAZ, while the influences of 100–300 mm/min welding speeds on the width of NZ are weak.
- (3) The hardness profiles of AA6061-T6 SSFSW joints show the softening regions located at the HAZ and TMAZ of both advancing side and retreating side. The lowest hardness value of joint reached 60% of the base metal hardness and the influence of 100–300 mm/min welding speeds on the hardness profile is more obvious than that of 750–1500 rpm tool rotation speeds.

- (4) The tensile strength of AA6061-T6 SSFSW joint increases with the increasing of the welding speed and is not sensitive to the tool rotation speed. The maximum and minimum tensile strength are 77.3% and 64.3% of the base metal strength for the welding parameters of 1500 rpm and 300 mm/min and 1500 rpm and 100 mm/min, respectively.
- (5) The fracture sites of AA6061-T6 SSFSW joint locate in the HAZ/TMAZ either on AS or RS and are affected by the tool rotation speed at the welding speed of 100 mm/min and not affected by the welding speed at the tool rotation speed of 1500 rpm. The fracture is dominated by a ductile transgranular characteristic.

References

- [1] Threadgill AJL PL, Shercliff HR, Withers PJ. Friction stir welding of aluminium alloys. *Int Mater Rev* 2009;54:49–93.
- [2] Gibson DHL BT, Prater TJ, Longhurst WR, Cox CD, Ballum MC, Dharmaraj KJ, et al. Friction stir welding: process, automation, and control. *J Manuf Proc* 2013.
- [3] Cui L, Yang X, Zhou G, Xu X, Shen Z. Characteristics of defects and tensile behaviors on friction stir welded AA6061-T4 T-joints. *Mater Sci Eng A* 2012;543:58–68.
- [4] Accera F, Buffa G, Fratini L, Troiano G. On the FSW of AA2024-T4 and AA7075-T6 T-joints: an industrial case study. *Int J Adv Manuf Technol* 2010;48: 1149–57.
- [5] Dharmawan F, Thomson RS, Li H, Herszberg I, Gellert E. Geometry and damage effects in a composite marine T-joint. *Compos Struct* 2004;66:181–7.
- [6] Fratini L, Buffa G, Filice L, Gagliardi F. Friction stir welding of AA6082-T6 T-joints: process engineering and performance measurement. *Proc Inst Mech Eng Part B – J Eng Manuf* 2006;220:669–76.
- [7] Russell MJ, Threadgill PL, Thomas MJ, Wynne BP. Static shoulder friction stir welding of Ti–6Al–4V; process and evaluation. In: 11th World Conference on titanium. Kyoto, Japan 2007.

- [8] Martin JP, Stanhope C, Gascoyne S. Novel techniques for corner joints using friction stir welding. TMS 2011 Annual Meeting & Exhibition. San Diego, (CA, USA): John Wiley & Sons, Inc.; 2011.
- [9] Tang W, Guo X, McClure J, Murr L, Nunes A. Heat input and temperature distribution in friction stir welding. *J Mater Process Manuf Sci* 1998;7:163–72.
- [10] Russell MJ and Blignault C. Recent developments in friction stir welding of Ti alloys. In: 6th International symposium on friction stir welding. Saint – Saveur, (Nr Montreal, Canada): Emerald Group Publishing Limited; 2006.
- [11] Ahmed BPW MMZ, Rainforth WM, Thredgill PL. Through-thickness crystallographic texture of stationary shoulder friction stir welded aluminium. *Scr Mater* 2011;64:45–8.
- [12] Davies PS, Wynne BP, Rainforth WM, Thomas MJ, Threadgill PL. Development of microstructure and crystallographic texture during stationary shoulder friction stir welding of Ti-6Al-4V. *Metall Mater Trans A* 2011;42:2278–89.
- [13] Widener CA, Talia JE, Tweedy BM, Burford DA. High-rotational speed friction stir welding with a fixed shoulder. In: 6th International symposium on friction stir welding; 2006.
- [14] Yu H. Welding Parameters, Distortion and mechanical properties of AA7075 lap joints in SSFSW. University of South Carolina; 2013.
- [15] Merlin A. Numerical and experimental investigation of friction stir welding: Politecnico di Milano; 2013.
- [16] Liu HJ, Li JQ, Duan WJ. Friction stir welding characteristics of 2219-T6 aluminum alloy assisted by external non-rotational shoulder. *Int J Adv Manuf Technol* 2013;64:1685–94.
- [17] Li JQ, Liu HJ. Effects of tool rotation speed on microstructures and mechanical properties of AA2219-T6 welded by the external non-rotational shoulder assisted friction stir welding. *Mater Des* 2013;43:299–306.
- [18] AW. Society, Specification for friction stir welding of aluminum alloys; 2010.
- [19] Liu H, Fujii H, Maeda M, Nogi K. Tensile properties and fracture locations of friction-stir welded joints of 6061-T6 aluminum alloy. *J Mater Sci Lett* 2003;22:1061–3.
- [20] Murr LE, Liu G, McClure JC. A TEM study of precipitation and related microstructures in friction-stir-welded 6061 aluminium. *J Mater Sci* 1998;33:1243–51.
- [21] Liu G, Murr LE, Niou CS, McClure JC, Vega FR. Microstructural aspects of the friction-stir welding of 6061-T6 aluminum. *Scr Mater* 1997;37:355–61.
- [22] Lee WB, Yeon Y-M, Jung S-B. Mechanical properties related to microstructural variation of 6061 Al alloy joints by friction stir welding. *Mater Trans* 2004;45:1700–5.
- [23] Woo W, Choo H. Softening behaviour of friction stir welded Al 6061-T6 and Mg AZ31B alloys. *Sci Technol Weld Joining* 2011;16:267–72.
- [24] Simar A, Bréchet Y, de Meester B, Denquin A, Pardoen T. Microstructure, local and global mechanical properties of friction stir welds in aluminium alloy 6005A-T6. *Mater Sci Eng A* 2008;486:85–95.
- [25] Woo W, Choo H, Brown D, Feng Z. Influence of the tool pin and shoulder on microstructure and natural aging kinetics in a friction-stir-processed 6061-T6 aluminum alloy. *Metall Mater Trans A* 2007;38:69–76.